ACS Catalysis

Research Article

pubs.acs.org/acscatalysis

O_2 Activation and Catalytic Alcohol Oxidation by Re Complexes with Redox-Active Ligands: A DFT Study of Mechanism

Shrabani Dinda,[†] Alexander Genest,[†] and Notker Rösch*[,†,‡]

[†]Institute of High Performance Computing, Agency for Science, Technology and Research, 1 Fusionopolis Way, #16-16 Connexis, Singapore 138632, Singapore

[‡]Department Chemie and Catalysis Research Center, Technische Universität München, 85747 Garching, Germany

Supporting Information

ABSTRACT: As a contribution to understanding catalysis by transition metal complexes with redox-active ligands (here: catecholate − cat), we report a computational study on the mechanism of a catalytic cycle where (i) O_2 is activated at the metal center of the catecholate complex $[Re^{V}(O)(cat)_2]^-$ to yield $[Re^{VII}(O)_2(cat)_2]^-$, which (ii) subsequently is applied to oxidize alcohols. We were able to identify the steps where the redox-active ligands played a crucial role as e^- buffer. For O_2 homolysis, a series of sequential $1e^-$ steps leads to superoxo and bimetallic intermediates, followed by facile cleavage of the bimetallic peroxo O−O linkage. The *trans*−*cis* isomerization of *trans*-$[Re^{V}(O)(cat)_2]^-$ is the crucial step of O_2 activation, with an absolute free energy barrier of 16.8 kcal mol^{-1} in methanol. Due to the ionic character of intermediates, all reaction barriers of O_2 activation are significantly lowered in a polar solvent, thus rendering O_2 homolysis kinetically accessible. With computational results for the activation barriers of all elementary steps as well as the calculated solvent effects, we are able to rationalize all pertinent experimental findings. For catalytic alcohol oxidation, we propose a novel cooperative mechanism that involves two units of the metal complexes, ruling out the reaction via a seven-coordinated active oxidant, as previously hypothesized. We present in detail calculated energies and barriers for the reaction steps of the oxidation of methanol as model alcohol as well as the energetics of crucial steps of the experimentally studied oxidation of benzyl alcohol, both transformations for methanol as solvent.

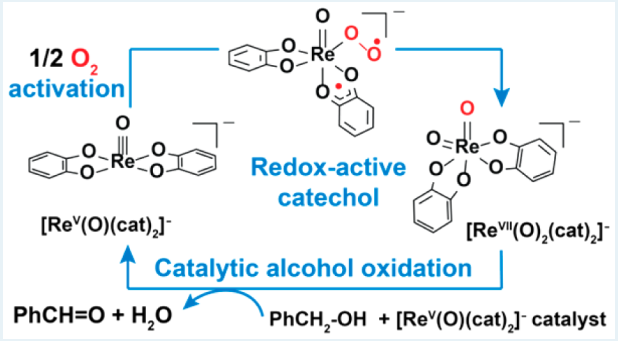

KEYWORDS: *O_2 homolysis, redox-active ligand, catalytic alcohol oxidation, oxorhenium complex, cooperativity within dinuclear complexes*

1. INTRODUCTION

Recently, redox-active ligands have attracted great interest for developing highly efficient and selective catalysts, where the transition metal center and the redox-active ligand cooperate in a synergistic manner.[1−6] A recent topical collection of articles on "cooperative and redox non-innocent ligands in directing organometallic reactivity"[7] is worth mentioning. Transformation of small molecules by redox-active transition metal catalysts to valuable chemicals via hydrogenation and dehydrogenation,[8−11] oxygenation,[12−14] C−C bond formation,[15,16] and C−H activation[17] has far-reaching applications, from pharmaceuticals to petroleum products. For the (partial) oxidation of organic substrates, molecular oxygen is an ideal "green" and inexpensive oxidant. The selective oxidation catalysis for both synthetic and biological systems by complexes with redox-active ligands is of timely interest.[18−22] Redox processes during O_2 activation, via $1e^-$ and $2e^-$ steps, at low-valent transition metal centers, to be transformed into high-valent metal−oxo intermediates, are well-known for the oxygenase enzyme chemistry.[20,23−25] Analogous 3d transition metal complexes may also serve as models for studying mechanistic details of enzyme catalysis.[23,26−31]

Computational studies are extremely useful for understanding the electronic structure and the spectroscopic properties of transition metal complexes with ancillary ligands of redox-active nature, as well as the role of their redox chemistry in various chemical reactions.[16,17,32−36] Particular noteworthy are extensive studies by Chirik and co-workers on pyridine-based pincer ligands of iron and cobalt complexes that facilitate C−C bond[37,38] formation and hydrogenation[11] because of their redox-active nature. Neese and co-workers applied Density Functional Theory (DFT) and *ab initio* methods for examining various trends in the experimental spectra of transition metal-complexes involving noninnocent ligands,[32] and for exploring systems of bioinorganic interest.[33,39]

Received: March 10, 2015
Revised: June 10, 2015
Published: July 23, 2015

DOI: 10.1021/acscatal.5b00509
ACS Catal. 2015, 5, 4869−4880

Recent experimental studies on the oxidation catalysis by the complex $[Re^{V}(O)(cat)_2]^-$ with redox-active catecholate ligands showed[12,40] the preparation of the higher-valent oxo transfer reagent $[Re^{VII}(O)_2(cat)_2]^-$ (Scheme 1). In the activation of oxygen, superoxo and peroxo intermediates are connected via a series of $1e^-$ steps. This superoxo species is trapped by a second anion $[Re^{V}(O)(cat)_2]^-$ to yield a dinuclear peroxo dianion complex. Finally, cleavage of the peroxo O−O bond yields the desired product $[Re^{VII}(O)_2(cat)_2]^-$, which contributes as oxo transfer reagent in the second half of the catalytic cycle (Scheme 2). The subsequent oxidation of alcohol is also catalyzed by $[Re^{V}(O)(cat)_2]^-$ (Scheme 1). There are quite a few examples for alcohol oxidation through O_2/peroxo-derived oxo transfer catalysis by transition metal complexes are known (e.g., oxo−vanadium,[41] oxo−molybdenum,[42,43] and oxo−rhenium).[44]

Scheme 1. O_2 Homolysis at $[Re^{V}(O)(cat)_2]^-$, Assisted by the Redox-Active Ligand Catechol, and Subsequent Catalytic Alcohol Oxidation[a]

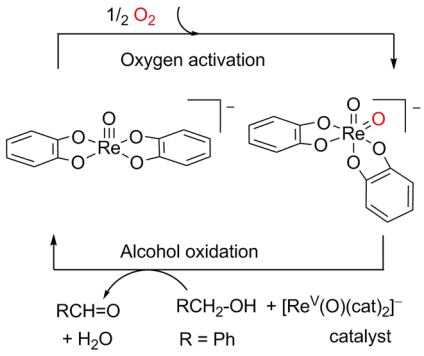

[a]Adapted from ref 12.

The characterization of the redox-active catecholate as electron-reservoir for O_2 homolysis was supplemented by computational studies.[40] Yet, several mechanistic details remained unclear, especially regarding the kinetics: (1) How does the *trans*−*cis* isomerization occur in the initial phase? (2) What is the role of O_2 during this isomerization? (3) How large is the activation barrier for forming the peroxo-bridged dimer? (4) What is the barrier for dissociating this dimer? (5) What is the impact of spin crossover on the overall kinetics? (6) What could be the role of the solvent?

Our computational study aims at examining all steps of the mechanism, including activation barriers, to answer these key questions and thus to offer a closer look at the experiments. Although there is some understanding regarding the role of redox-active ligands in the hemolysis of O_2, to the best of our knowledge, there is no computational study about the catalytic oxidation of alcohols by Re complexes (the second half of the reaction), especially whether redox-active ligands have any role to play. A hydroxo−alkoxo rhenium(VII) complex, generated *in situ* by intramolecular delivery of an alcohol (ROH, R = Me, benzyl) from $[Re^{V}(O)(ROH)(cat)_2]^-$ to $[Re^{VII}(O)_2(cat)_2]^-$, has been suggested as active oxidant.[12] Formally, net H_2 addition from an alcohol to $[Re^{VII}(O)_2(cat)_2]^-$ via proton-coupled electron transfer (PCET) produces the aldehyde and a $[Re^{V}(O)(cat)_2]^-$ complex. Exploring the mechanism in the spirit of computational catalysis is extremely important for understanding the experiments, particularly the chemistry behind the hypothesis of hydroxo−alkoxo Re^{VII} as active oxidant. Experimentally, the oxidation of benzyl alcohol was traced to the formation of benzaldehyde, but no clear product was determined in the case of methanol oxidation.[12] As all species involved are ionic, one may anticipate effects of polar solvents, like methanol or acetonitrile, used as reaction media in experiment, on the thermodynamics as well as the reaction kinetics.

The present mechanistic investigation, based on DFT calculations, will reveal a scenario of the full catalytic cycle and provide substantial insight into the reaction mechanism. Regarding the involvement of radicals and the association of mononuclear species to yield dinuclear complexes, special care has been taken to calculate the energetics. As to the alcohol oxidation, we will first describe calculations on methanol oxidation, followed by a brief discussion of the oxidation of benzyl alcohol.

2. RESULTS AND DISCUSSION

2.1. Conversion of $[Re^{V}(O)(cat)_2]^-$ to $[Re^{VII}(O)_2(cat)_2]^-$ by Aerial O_2. The activation of O_2 at the Re center of $[Re^{V}(O)(cat)_2]^-$ **1** to produce the higher-valent substrate $[Re^{VII}(O)_2(cat)_2]^{2-}$ comprises three main phases (Scheme 3): addition of O_2, formation of a peroxo dimer, and cleavage of

Scheme 2. Simplified Scheme of Alcohol Oxidation[a]

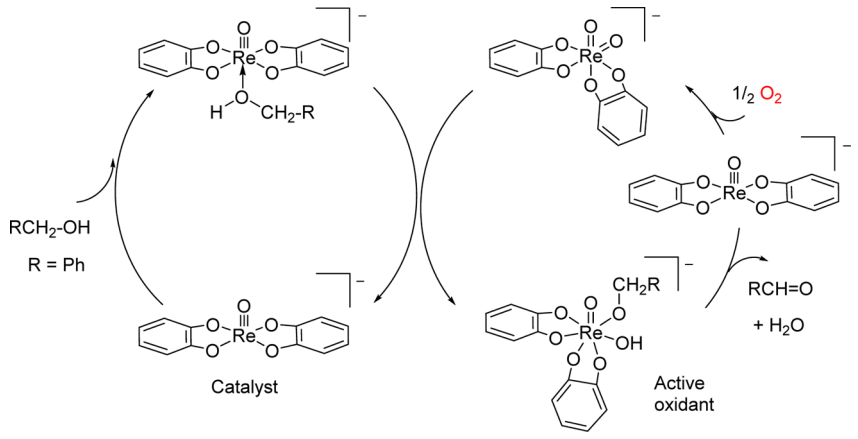

[a]Adapted from ref 12.

DOI: 10.1021/acscatal.5b00509
ACS Catal. 2015, 5, 4869−4880

Scheme 3. Detailed Mechanistic Scheme of O_2 Activation at $[Re^{V}(O)(cat)_2]^-$, Assisted by Redox-Active Ligands Catechol, Reporting the Calculated Reaction Free Energies (Black) and Activation Barriers (Red) Determined in This Work[a]

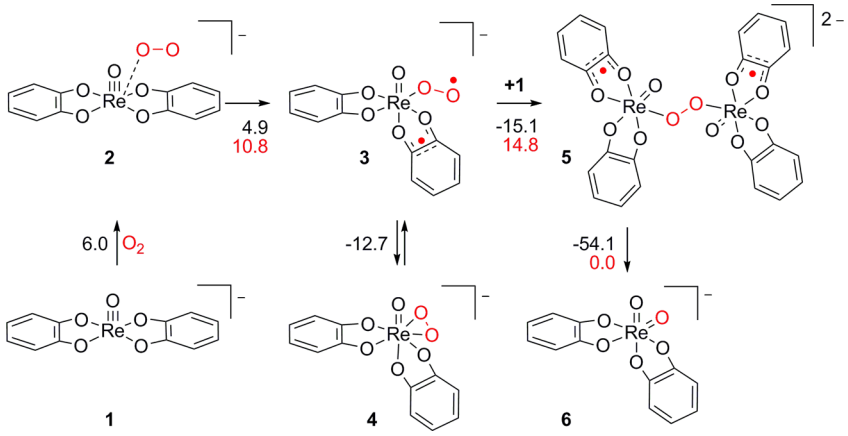

[a]See Section 2.1. Energies in kcal mol^{-1}.

the peroxo O–O linkage. Figure 1 shows the calculated Gibbs free energy profile for this transformation, as it is taking place in

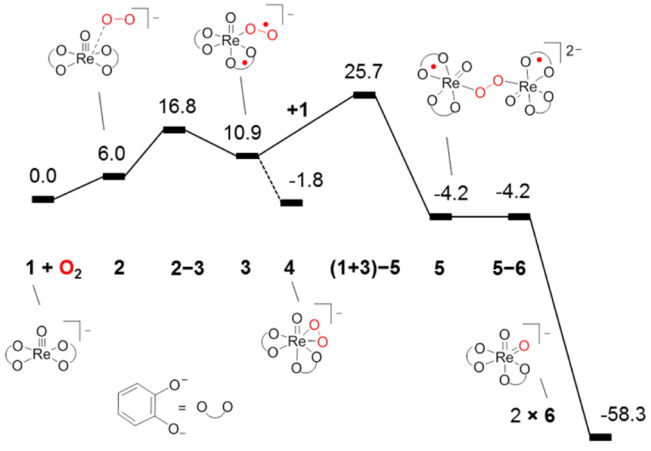

Figure 1. Free energy profile (kcal mol^{-1}) of O_2 activation in methanol, assisted by redox-active catechol ligands of the complex $[Re^{V}(O)(cat)_2]^-$. The species **1**, **4**, and **6** are in singlet configuration, and all other compounds and transition states are in triplet configuration; see Scheme 3.

methanol as solvent. These computational results corroborate a facile radical pathway for O_2 activation, as previously proposed on the basis of experimental findings.[40]

The entropy correction applied is described in Section 4.2, Computational Details. Figure S1 of the Supporting Information (SI) provides comparative energy profiles for systems in the gas phase and in methanol. The underlying electronic energies, corrected for zero-point energies, and the Gibbs free energy values, both in the gas phase and in methanol, are tabulated in Table S1 of the SI. As the overall reaction involves a charge separation, profound solvent effects are observed.

2.1.1. Addition of O_2. The transformation of *trans*-$[Re^{V}(O)(cat)_2]^-$ **1** to the final product *cis*-$[Re^{VII}(O)_2(cat)_2]^-$ **6** implies a *trans*–*cis* rearrangement of the cat ligands during O_2 activation. The addition of O_2 to **1** has been suggested to involve an isomerization of the more stable *trans* isomer to the less stable *cis* conformer of **1**,[40] yet details remained open. Among others, we also explored computationally adding O_2 to the Re center in end-on *trans* fashion, but only the end-on *cis* approach yielded the desired synchronous *trans*–*cis* isomerization process with a low barrier. Our calculations show that an end-on approach of O_2 toward the Re center of **1** induces a *synchronous* change of the conformation, from *trans* to *cis*, with a notably lower activation barrier, E_a = 10.8 kcal mol^{-1} (Figure 1). The triplet adduct **2**, formed as an association of **1** and O_2, is slightly higher in energy, by 6.0 kcal mol^{-1} compared to the starting molecules at formally infinite separation (Figure 1). A detailed description of **2** and the optimized structures of all intermediates are provided as SI; see Sections S2 and S3.

In TS **2**–**3**, the *cis* approach of incoming O_2 with respect to the Re–oxo bond is responsible for the stated *trans*–*cis* isomerization of **1**. Along the reaction path from **2** to TS **2**–**3**, the Re–O(oxo) distance is reduced from 416 to 248 pm (Figure 2). Simultaneously the angle O(oxo)–Re–O(cat) changes from 110° to 142°, clearly illustrating the torsional flexibility of the ligand liable for the *trans*–*cis* isomerization. The absolute energy of product **3**, a triplet diradical complex, is 10.9 kcal mol^{-1} (Figure 1). The analogous *trans* approach does not lead to an isomerization and the resultant intermediate, an isomer of **3**, is calculated 12 kcal mol^{-1} above **3**.

From a Mulliken population analysis of the singly occupied molecular orbitals (SOMOs), one is able to formulate the triplet diradical characteristics of **3** as $[Re^{V}(O)(O_2^{\bullet-})(cat)(sq^{\bullet-})]^-$, with a reduced η^1-superoxo $O_2^{\bullet-}$ ligand and a partially reduced semiquinone radical $sq^{\bullet-}$ (Figure 3), confirming an earlier assignment.[40] A population analysis of the spin density reveals that one spin is distributed over the dioxygen moiety in which the distal oxygen center shares 68% of the total spin. The second unpaired spin is spread over the Re center (49%) and one of the catecholate ligands (Figure S4 of SI). In this 1e$^-$ oxidation–reduction process **2** → **3**, the redox-active ligand is oxidized, cat → $sq^{\bullet-}$ while O_2 is reduced according to O_2^0 → $O_2^{\bullet-}$. In the analogous singlet species $[Re^{VII}(O)(O_2^{2-})(cat)_2]^-$ **4**, the peroxo ligand is linked to the metal center in η^2 fashion (Figure S3 of SI). Significant structural differences between the species **3** and **4** are notable as variations in the distances Re–O and O–O, as well as the angle Re–O–O. In the triplet species, these parameters are Re–O = 206 pm, 288 pm, O–O = 132 pm, and Re–O–O = 115°, whereas the singlet species are characterized by Re–O = 194 pm, 204 pm, O–O = 143 pm, and Re–O–O = 72° (Figure S3

DOI: 10.1021/acscatal.5b00509
ACS Catal. 2015, 5, 4869–4880

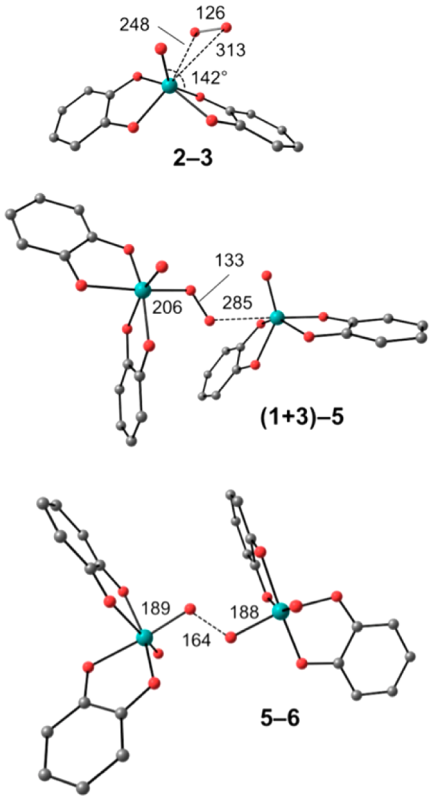

Figure 2. Optimized structures of the TSs involved in the homolysis process of O_2 at the Re center of **1**; selected bond distances in pm. Noninteracting hydrogen atoms are omitted for clarity.

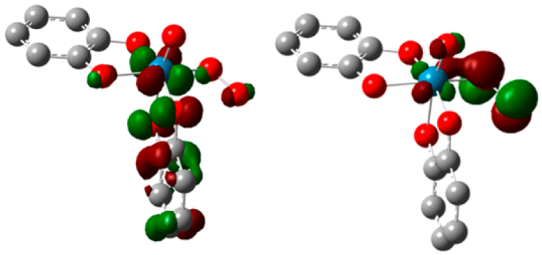

Figure 3. Singly occupied molecular orbitals (SOMOs) of complex **3**.

of SI). The triplet-to-singlet isomerization **3** → **4** is exergonic by 12.7 kcal mol^{-1} in methanol (Figure 1).

2.1.2. Spin Crossover. In the superoxo-to-peroxo transformation **3** → **4**, formally a $1e^-$ redox step, a second transition metal−oxygen bond is formed. This type of reaction is well-known for many transition metal complexes (e.g., of Cu,[45−47] and Pd).[48−50] The conversion of the triplet state **3** to the singlet state **4** requires an intersystem crossing.

To locate approximately the structures where the spin crossover may occur, we scanned the potential energy surfaces of both spin states at various fixed Re−O (distal) distances in the spirit of the minimum energy crossing point method.[51] For a given Re−O constraint, we optimized the structure of both spin states and thus determined an approximate intersection of the two potential energy surfaces near Re−O = 258 pm (Figure 4). The corresponding singlet and triplet structures are rather similar (Figure S5 of SI). For the systems in the gas phase, this approximate crossing point has a zero-point corrected electronic energy that is by ∼3.0 kcal mol^{-1} higher than that of the triplet structure **3**. In the singlet state, the peroxo ligand

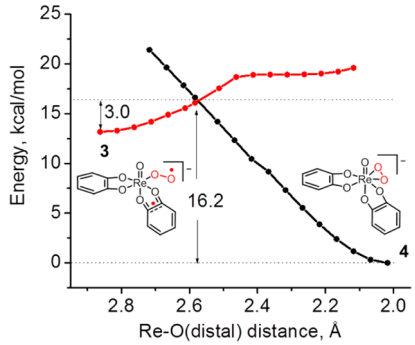

Figure 4. Singlet and triplet energy profiles for the second Re−O binding in $[Re(O)(O-O)(cat)_2]^-$. The energies are zero-point corrected electronic energies for systems in the gas phase.

is characterized by Re−O = 195 pm, 258 pm, O−O = 139 pm, and Re−O−O = 100°; the corresponding structural parameters in the triplet state are Re−O = 204 pm, 258 pm, O−O = 132 pm, and Re−O−O = 98°. This close similarity of the geometries between the singlet and triplet state structures near the singlet−triplet crossing point further suggests an easy spin crossover, to be mediated by spin−orbit interaction which generally is large for third-row transition metals like Re.[52] This transformation is further facilitated by the fact that two unpaired spins are quite delocalized; see the SOMOs in Figure 3. Therefore, the exchange interaction is weakened.

The results for the present Re complex are quite similar to those for the well-known Cu and Pd systems with d^{10} centers,[45,50] where spin crossover was seen to be facilitated by a weak exchange interaction. This weakened exchange interaction has also previously been postulated for a Re-oxo complex.[40]

2.1.3. Formation of a Peroxo-Linked Dimer and Cleavage of the Peroxo Bond. Once the superoxo monomer **3** has been formed, the next step in the catalytic cycle (Scheme 3) is the formation of the dinuclear metal complex **5** via interaction of the highly reactive triplet diradical **3** with another molecule of **1**. Complex **5** contains a trans-μ-1,2-peroxo O_2^{2-} linkage. We were able to locate the minimum energy structures of both spin states of **5**, which were quite similar to the structures reported earlier.[40] In both cases, we also determined symmetric charge distributions and comparable geometric parameters[40] of the two fragments $[Re(O)(cat)_2]^-$. With the $1e^-$ oxidation of the second $[Re(O)(cat)_2]^-$ fragment, which contains the partially oxidized ligand $sq^{\bullet-}$, it seems appropriate to interpret the electronic structure of **5** as $[(cat)(sq^{\bullet-})(O)Re-O-O-Re(O)(cat)(sq^{\bullet-})]^{2-}$. In methanol solution, the triplet state of dimer **5** is by 17.3 kcal mol^{-1} more stable than the corresponding closed-shell singlet state of **5**. The two spin states feature slightly different structures. For example, the alignment of the ligands is characterized by dihedral angles (oxo)O−Re−Re−O(oxo) of −165° in the triplet state and −133° in the singlet state (Figure S3 of SI). In the triplet state, the two $[Re(O)(cat)(sq^{\bullet-})]^-$ moieties of **5** are aligned in a parallel fashion; each of them carries one spin (Figure S6a of SI), distributed in similar fashion over the Re center and the $sq^{\bullet-}$ moiety (Figure S6b of SI).

The activation barrier of (**1** + **3**) → **5** toward the formation of the dimer **5** in methanol is calculated at 14.8 kcal mol^{-1} (Figure 1) with respect to the triplet superoxo species **3** and complex **1** at formally infinite separation. As in the preceding first step **2** → **3** during the O_2 attack at *trans*-$[Re(O)(cat)_2]^-$, a

DOI: 10.1021/acscatal.5b00509
ACS Catal. 2015, 5, 4869−4880

Scheme 4. Mechanistic Scheme Studied for the Alcohol Oxidation by Rhenium Catechol Complexes on the Example of Methanol[a]

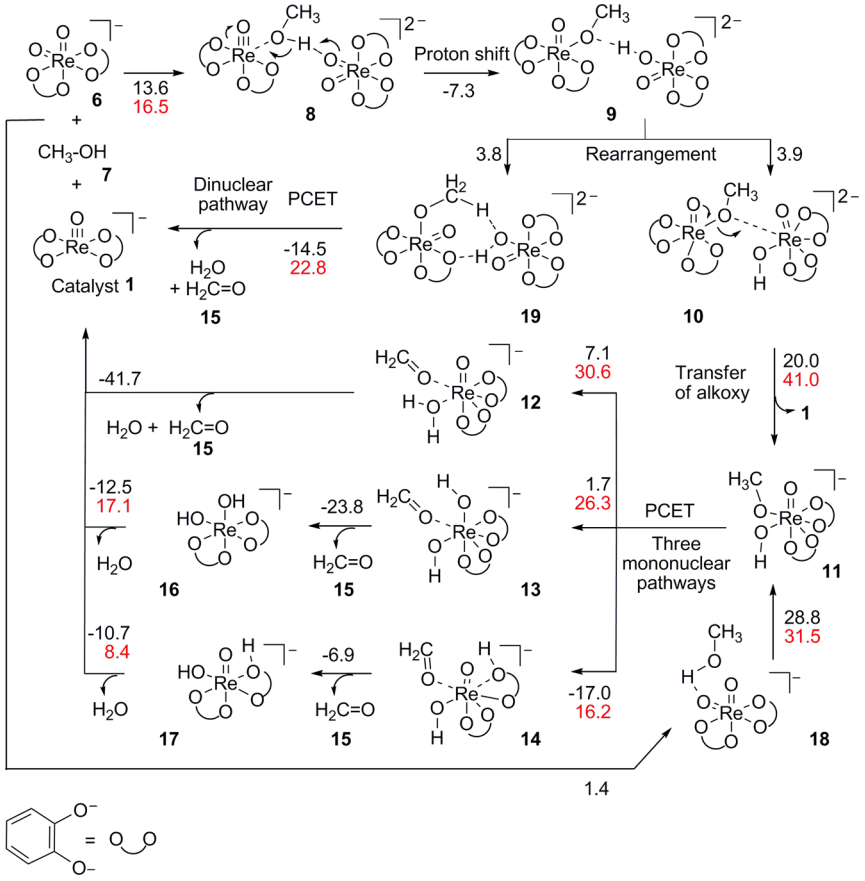

[a]The complexes **9**, **10**, and **19** are in a triplet state. The reaction free energies and activation barriers (in kcal mol^{-1}) are shown in black and red, respectively.

similar *trans*−*cis* isomerization is determined when the superoxo complex **3** approaches *trans*-$[Re(O)(cat)_2]^-$ **1**. The TS (**1** + **3**)−**5**, and the resulting dinuclear intermediate **5** involve a radical reaction (Scheme 3). For species in the gas phase, that relative barrier is extremely high, 63.3 kcal mol^{-1} (Figure S1 of SI). This very unfavorable energetics in the gas phase is to be expected because two negatively charged species are approaching each other, encountering a notable Coulombic repulsion.

The free energy reaction profile changes substantially for reactions in methanol (Section S1 of SI). The relative energies, with respect to the starting materials 2 × **1** + O_2, of these configurations are quite substantially lowered, by 52.9 kcal mol^{-1} for the intermediate **5**, by 50.5 kcal mol^{-1} for the TSs for the reaction (**1** + **3**) → **5**, and by 53.8 kcal mol^{-1} for the TSs of **5** → 2 × **6**. The estimated relative activation barrier for the association (**1** + **3**) → **5** is thus dramatically reduced, from 63.3 kcal mol^{-1} in the gas phase to 14.8 kcal mol^{-1} in methanol. The subsequent dissociation step **5** → **6** is calculated to be almost without barrier, 0.9 kcal mol^{-1} and 0.0 kcal mol^{-1}, in the gas phase and in methanol, respectively.

In methanol, both processes, the O_2 attack **2** → **3** and the formation (**1** + **3**) → **5** of the dinuclear intermediate **5**, have comparable relative barriers, 10.8 kcal mol^{-1} and 14.8 kcal mol^{-1}, respectively. These two calculated barrier values are sufficiently similar to agree qualitatively with the experimental kinetics data[40] that implied the conversion (**1** + $\mathbf{O_2}$) → **6** to proceed over two consecutive barriers of comparable heights.

The homolytic O−O bond cleavage in **5** leads to two species of the final Re^{VII}−dioxo product $[Re(O)_2(cat)_2]^-$ **6**. This reaction implies 1e$^-$ redox processes where the electron transfer takes place from each fragment of $[Re(O)(cat)(sq^{\bullet-})]$ to O_2^{2-}. The TS **5**−**6** involved has almost no barrier relative to **5** (Figure 1). The normal mode across the barrier corresponds to the breaking of the peroxo link and yields two diradical fragments $[Re(O)(O^{\bullet})(cat)(sq^{\bullet-})]^-$. The two unpaired e$^-$, one on O$^{\bullet}$ and the other one on the moiety $[Re(sq^{\bullet-})]$, pair to yield two units of the singlet complex $[Re(O)_2(cat)_2]^-$ **6**. The open-shell singlet of the dinuclear species **5** is estimated to be only 0.7 kcal mol^{-1} higher in energy (Section 4), providing yet another hint for a facile triplet-to-singlet crossover. The reaction **5** → 2 × **6** is highly exergonic, with a change in free energy of −54.1 kcal mol^{-1} in methanol (Figure 1).

2.2. Alcohol Oxidation Catalyzed by a Rhenium Oxo Complex. The first half of the catalytic cycle (Scheme 2) describes the preparation of the higher-valent oxidative substrate $[Re^{VII}(O)_2(cat)_2]^-$ **6** as oxo transfer reagent in the second half of the cycle where an alcohol is oxidized to its corresponding aldehyde. The oxidation of the alcohol is accompanied by a reduction of **6** to the Re^{V} species **1** which also acts as catalyst for this reaction. When exploring the reaction mechanism, we will first report our effort to probe the original hypothesis[12] that the hydroxo−alkoxo Re^{VII} moiety **11**

DOI: 10.1021/acscatal.5b00509
ACS Catal. 2015, 5, 4869−4880

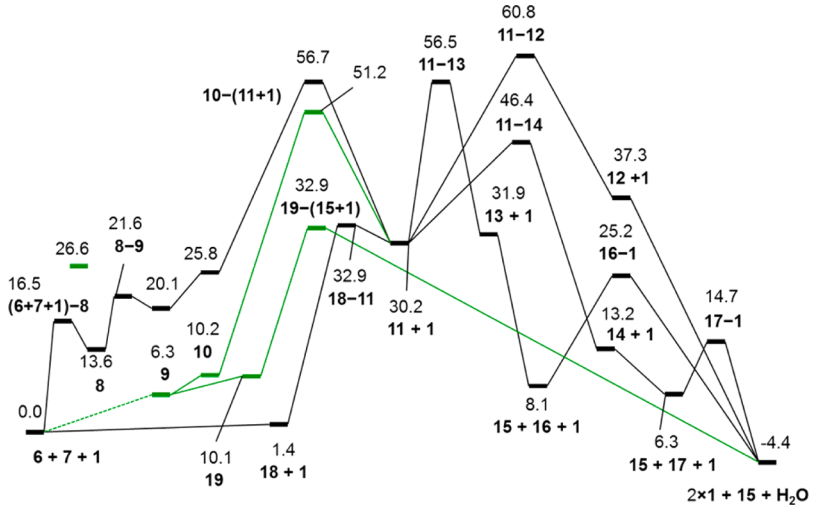

Figure 5. Free energy profile (kcal mol^{-1}) for the oxidation of methanol by rhenium catechol complexes (Scheme 4). The black lines indicate the singlet pathway; triplet states are given in green.

is the active oxidant. We examined two pathways for forming the seven-coordinated hydroxo−alkoxo Re^{VII} complex **11**, Scheme 4. (i) Along a "dinuclear" path, the association of substrate methanol **7** to the dimer formed by the oxidant **6** and the catalyst **1** yields the dinuclear complex **9**, from which complex **11** emerges after alkoxy transfer and an expulsion of one instance of species **1** (Section 2.2.1). (ii) Along a "monoculear" pathway, substrate **7** binds to the oxidant **6** and, after transfer of an alkoxy moiety, rearranges to complex **11** (Section 2.2.2). From **11**, via intramolecular PCET, three routes seem plausible for reaching the aldehyde **15** and an instance of complex **1** (Section 2.2.3). Finally, as most favorable alternative, we present a "direct" pathway, via the dinuclear complex **9**, that runs exclusively on the triplet potential energy surface, to yield product **15** and two instances of the Re^{V} complex **1** (Section 2.2.4).

Initially, we explored the reaction mechanism using methanol as model alcohol. Figure 5 shows the resulting free energy profile for systems solvated in methanol. Optimized structures and geometrical parameters of all the intermediates are provided as SI; see Figure S7. The structures of the various transition states are shown in Figure 6. The zero-point corrected relative electronic energies and Gibbs free energies for systems, both in the gas phase and in methanol, are collected in Table S2 of the SI.

Later on, we will elaborate some variations associated with benzyl alcohol as substrate, because both substrates have experimentally been studied.[12]

2.2.1. Formation of the Seven-Coordinated Hydroxo−Alkoxo Re^{VII} Complex 11 via Dinuclear Intermediate 9. Under experimental conditions,[12] where a mixture of Re^{VII} **6**, methanol **7** and a catalytic amount of Re^{V} **1** are present in the reaction medium, initially the alcohol may coordinate to the lower coordinated Re^{V} center of **1** via oxygen (Scheme 2).[12] The vacant coordination site in **1**, *trans* to the axial Re−oxo bond, provides room for the incoming alcohol. It was previously reported[12] that isomerization of the *trans* isomer is preferred at Re^{V} for ligands that are π-acids, such as O_2 or PPh_3. The structure with methanol coordinated in *cis* fashion to the Re^{V} center of **1** is only by 5 kcal mol^{-1} higher in energy than the complex with methanol in *trans* coordination.[53] As a result, there will be a *trans*-to-*cis* isomerization of the catecholate ligands. In the presence of a further ligand, such structural flexibility of **1** is quite feasible; see Section 2.1.1. The formation of the hydroxo−alkoxo Re^{VII} complex **11**[12] involves a proton transfer from the alcohol coordinated to complex **1** (Scheme 4) to an oxo group. The dinuclear adduct **8** offers an ideal arrangement for this intramolecular proton shift. The alcohol binding in **8**, Re−O = 227 pm, is coupled with a hydrogen bond between the −OH group of the alcohol and an oxo moiety of **6**, OH−O = 173 pm (Scheme 4, Figure S7 of SI). In methanol, this step (**6** + **7** + **1**) → **8** is endergonic by 13.6 kcal mol^{-1} (Figure 5). The corresponding activation barrier, 16.5 kcal mol^{-1}, which includes a *trans-cis* isomerization, is notably higher than the activation barrier for a similar isomerization step, triggered by a π-acid ligand like O_2, 10.8 kcal mol^{-1} (reaction **2** → **3**). As expected from our previous observation for (**1** + **3**) → **5**, Section 2.1.3, a significant solvation effect is determined (Table S2 of SI) as two negatively charged species **1** and **6** combine to yield the dianionic dinuclear complex **8**.

The singlet Re dimer **9** results after an intramolecular proton shift via a relative barrier of 8 kcal mol^{-1} (Figure 5). The newly formed alkoxy and hydroxy groups of **9** are coordinated each to one of the Re centers, Re−O = 200 and 190 pm, where a strong hydrogen bond, MeO−HO = 156 pm, holds the two metal units together (Scheme 4, Figure S7 of SI). Such dinuclear Re complexes, bridged by hydrogen bonding, are well-known.[54] Reaction **8** → **9**, is slightly endergonic, by 6.5 kcal mol^{-1}, and the relative activation barrier is calculated at 8.0 kcal mol^{-1} in methanol (Figure 5). The imaginary vibrational mode of TS **8**−**9** is related to an increase in the alcoholic O−H distance to 133 pm and a decrease in oxo−H to 110 pm, compared to **8** (Figure 6).

The intramolecular migration of the methoxide ($-OCH_3$) moiety of complex **9**, from one Re center to the other, is essential for obtaining the seven-coordinated oxidant **11**. The MeO−HO hydrogen bond in **9** renders this migration even more difficult, in addition to the fact that already the octahedral metal center is coordinatively saturated. We calculated the resulting intermediate **10** slightly higher in free energy, by 5.7 kcal mol^{-1} (Scheme 4, Figure 5). Complex **10** acts as starting point for the intramolecular migration of methoxide (Scheme 4). The large separation, 333 pm, between the oxygen and the hydrogen centers of $-OCH_3$ and −OH in **10** (Figure S7 of SI),

DOI: 10.1021/acscatal.5b00509
ACS Catal. 2015, 5, 4869−4880

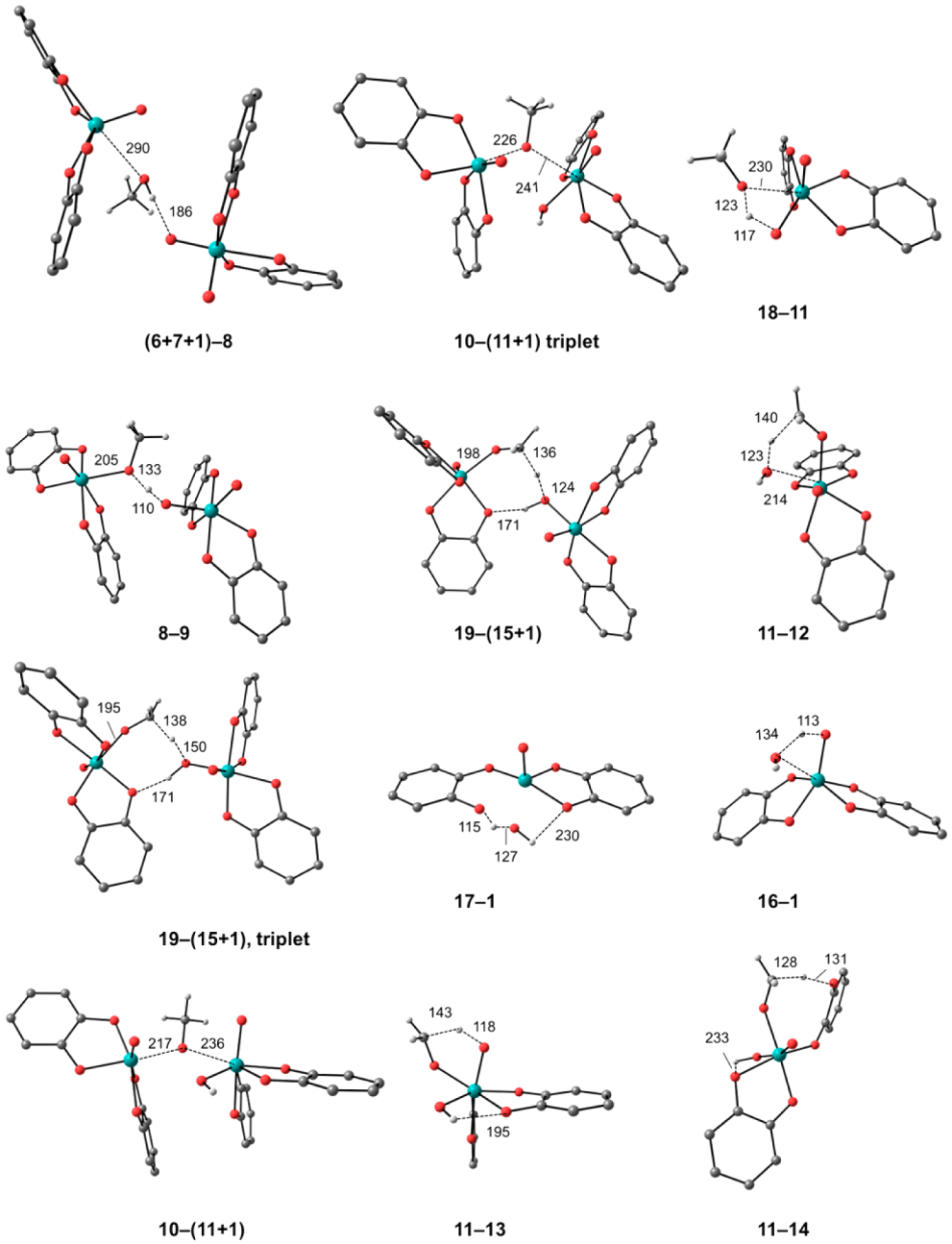

Figure 6. Optimized structures of the TSs involved in the alcohol oxidation process with important bond distances in pm. Noninteracting hydrogen atoms are omitted for clarity.

paves the way for the alkoxy migration, an uphill process with a relative free energy barrier of 30.9 kcal mol^{-1} (Figure 5). The Re−OCH_3 distances in TS **10**−(**11** + **1**) are 217 and 236 pm (Figure 6). As product of this migration, one regenerates the catalyst **1** and obtains the seven-coordinated oxidant **11** where both −OCH_3 and −OH are coordinated to the Re^{VII} center, as proposed by an experimental study.[12] Two comments are in order. (i) The absolute barrier of TS **10**−(**11** + **1**) is quite high, 56.7 kcal mol^{-1} above the initial compounds **6** + **7** + **1**. (ii) The formation of intermediate **11** is very endergonic, by 30.2 kcal mol^{-1} relative to **6** + **7**, rendering this intermediate not very likely along the reaction path of alcohol oxidation.

Unlike for the homolysis of O_2 (Section 2.1), the experimental works do not address any radical intermediates for the alcohol oxidation process,[12] although both complexes **1** and **6** include the redox-active ligand catechol. Our calculations suggest (Figure 5, Table S2 of SI) that the relative energies of the triplet dinuclear complexes are significantly lower compared to their pertinent singlet complexes, except for species **8**, which is only a very weekly bound adduct of **1**, **6**, and **7**. The triplet dinuclear complexes **9** and **10** are stabilized compared to their singlet analogues by 13.8 kcal mol^{-1} and 15.6 kcal mol^{-1}, respectively, whereas the triplet TS **10**−(**11** + **1**) is only 5.5 kcal mol^{-1} lower in energy than its singlet congener, with an absolute free energy barrier of 51.2 kcal mol^{-1} on the triplet potential energy surface (Figure 5). This extremely high barrier for a reaction at ambient temperature[12] prompted us to search for a lower lying path to intermediate **11**; see Section 2.2.2.

We conclude this section by a comment on the formation of intermediate **9** in the triplet state. Once **9** has been formed, a

DOI: 10.1021/acscatal.5b00509
ACS Catal. 2015, 5, 4869−4880

direct singlet-to-triplet spin crossover may occur. However, it more likely is a spin crossover that occurs synchronously with the proton shift, **8** → **9**. The spin density distribution and the general MO analysis of complex **9** (Figure S8 of SI) are indicative of the diradical nature of complex **9**, with one unpaired e^- located each at the Re (∼60%) and a catechol ligand (∼30%). This electronic structure is quite similar to that of the dinuclear complex **5** (Section 2.1.3). Typically, the redox-active ligand catechol may act as e^- buffer by transforming into a partially oxidized moiety $sq^{\bullet -}$.

*2.2.2. Formation of the Hydroxo−Alkoxo Re^{VII} Complex **11** without Catalyst **1**.* The high barriers, just discussed, essentially ruled out the intramolecular transfer of the alkoxy group via catalyst **1** to yield complex **11**. Note that intermediate **11** is an isomer of the adduct **18** (Scheme 4), formed by oxidant **6** and substrate **7**. This reaction is very slightly endergonic, by only 1.4 kcal mol^{-1} (Figure 5). In adduct **18**, the two constituents **6** and **7** interact by a hydrogen bond via the alcoholic OH and an oxo−Re moiety, with OH−O(Re) = 185 pm (Figure S7 of SI). The subsequent TS **18**−**11** (Figure 6) involves the migration of the alcoholic hydrogen to the oxo group, RO−H = 123 pm and ReO−H = 117 pm, and a simultaneous coordination of the methoxy group to the Re center, Re−OCH_3 = 230 pm (Figure 6). Most importantly, the absolute activation barrier **18** → **11**, 32.9 kcal mol^{-1} (Figure 5), is much lower than the absolute barrier **10** → (**11** + **1**), 51.2 kcal mol^{-1}, for the alkoxy transfer in the triplet state (Section 2.2.1). Given the very low lying initial state **18** and the much lower barrier of **18** → **11**, intermediate **11** will preferentially be formed via this "mononuclear", and not the "dinuclear" pathway via **9** and **10** on the triplet potential energy surface. This "mononuclear" alternative path renders the high-lying intermediate **11** more accessible, but is at variance with the experimentally found dependence of the reaction on the presence of the Re^V compound **1**.[12]

*2.2.3. Aldehyde Formation from the Hydroxo−Alkoxo Re^{VII} Complex **11**.* Although the crucial intermediate **11** lies already rather high in energy (Figure 5), we explored the remaining part of the reaction network (Scheme 4), because the hypothesis of a mononuclear PCET process was formulated in the experimental work.[12] Starting from **11** and following a PCET mechanism,[12] a reduction of the Re^{VII} moiety and a simultaneous oxidation of the alkoxy species will ultimately yield the aldehyde **15** and regenerate the Re^V complex **1** (Scheme 4). Overall, this transformation implies a net transfer of $2e^-$ from the alkoxy species to the Re^{VII} center, via oxy/oxo ligands. In complex **11**, a proton can be transferred to one of the three oxy/oxo groups present, namely, the rhenium−oxo, hydroxy, and catecholate oxy groups. All complexes discussed in the following have a closed-shell electronic structure.

Out of these three plausible pathways, proton transfer to the hydroxyl group via the five-member TS **11**−**12** had previously been suggested.[12] In that TS, the alkoxy C−H bond was calculated to increase from 110 to 140 pm (Figure 6); concomitantly, the H−OH distance decreases from 235 to 123 pm. The relative activation barrier for this step **11** → **12** is calculated at 30.6 kcal mol^{-1} (Figure 5). Similarly high relative energy barriers have previously been determined when alcohols are oxidized to aldehydes by d^0 transition metal−oxo complexes.[55] The resultant product adduct **12** includes both **15** and a water molecule in the second coordination shell of the Re^V center, with Re−O = 202 pm, 218 pm (Figure S7 of SI). Removal of the aldehyde and the aqua ligand in the final stage yields catalyst **1**; this process is exergonic by −41.7 kcal mol^{-1} (Figure 5). Although the overall process **11** → **1** + **15** + H_2O is exergonic by −34.6 kcal mol^{-1}, this path has to be ruled out in view of the high absolute barrier of **11** → **12**, 60.8 kcal mol^{-1} (Figure 5).

The alternative proton transfer **11** → **13** to the rhenium−oxo group via a five-member TS results in the dihydroxyl−rhenium−catecholate complex **13** (Scheme 4) with a loosely bound aldehyde, at Re−O = 213 pm (Figure S7 of SI). Along this path, the product **15** is first removed from **13**, leading to the dihydroxy complex **16**, which eliminates an aqua ligand to regenerate **1** (Figure 5). Yet, also this path is very unlikely as the relative activation barrier, 26.3 kcal mol^{-1}, is only 4.3 kcal mol^{-1} lower, than for the PCET reaction **11** → **12**.

The third alternative **11** → **14** (Figure 5), namely, proton abstraction by one of the catecholate oxy group, is rather an easy process, with a relative activation barrier of only 16.2 kcal mol^{-1} (Figure 5). During this process, structural strain is released as the coordination number of the Re center changes from seven to six; the catecholate loses one of its O−Re bonds due to protonation. The product **14** is a hexa-coordinated complex with loosely bound aldehyde **15** in the second coordination shell, Re−O = 215 pm, and newly formed catecholate hydroxyl group −OH, which binds via its hydrogen to the hydroxyl at the Re center, with H−O = 162 pm (Figure S7 of SI). In the subsequent step, aldehyde **15** is released and intermediate **17** is formed, which affords easy removal of an aqua ligand, with a barrier of 8.4 kcal mol^{-1}, finally to regenerate catalyst **1**.

In addition, we also probed proton shuttling via an extra molecule of methanol in the model, located between the alkoxy and the oxy/oxo groups. The calculated energetics was not significantly improved; rather, the activation barriers increased by 1−9 kcal mol^{-1}.

In summary, the proton shift **11** → **14** to the catecholate oxy moiety is preferred, but the absolute barrier, 46.4 kcal mol^{-1} above **1** + **6** + **7**, renders also this pathway as incompatible with the observed easy reaction at room temperature.[12]

2.2.4. Direct Aldehyde Formation via the Dinuclear PCET Pathway. These negative results prompted our further search for an alternative mechanism that avoids intermediate **11**. In fact, prior to the formation of **11**, alcohol oxidation may take place via a pathway involving a PCET step starting from the dinuclear complex **9**. Therefore, we refer to this alternative as "dinuclear PCET" pathway (Scheme 4).

A suitable CH−O interaction seems to be favorable for extracting a hydrogen from the carbon center, to form ultimately the aldehyde **15**. Therefore, we examined the adduct **19**, a nearly iso-energetic isomer of **10**, as potential precursor of alcohol oxidation. As the triplet states of dinuclear complexes are lower in energy than the corresponding singlet species (Section 2.2.1), the following discussion addresses the potential energy surface of *triplet* states, unless stated otherwise.

Minor structural rearrangements of **9**, like a change in the hydrogen bonding and CH−O type interactions, lead to the nearly iso-energetic intermediate **19** (Figure 5) where ancillary ligands around the two Re centers perfectly set the stage for the transfer of an alkoxy proton to a hydroxy group (Scheme 4). The slightly different alignment of the ligands in the two dinuclear complexes is manifest in the dihedral angles (oxo)O−Re−Re−O(oxo): −22° in **9** and 83° in **19** (Figure S7 of SI). However, the electronic structure of these two complexes remains quite similar, regarding both the character of the two

DOI: 10.1021/acscatal.5b00509
ACS Catal. 2015, 5, 4869−4880

SOMO pairs and the associated spin densities. In complex **19**, one may distinguish the following interactions (Figure S7 of SI): (i) hydrogen bonding between a hydroxyl moiety −OH and one of the catecholate oxygen centers of the other Re center, OH−O = 198 pm, (ii) a CH−O type interaction, at 293 pm, between a CH moiety of a methoxy and a hydroxyl moiety, and (iii) a CH−O type interaction, at 264 pm, between a CH of catecholate and an oxy center of a catecholate at the second Re center. In the TS **19**−(**15** + **1**), the Re center, the alkoxy group (O−C), the hydroxyl (O−H), and the catecholate O maintain a nearly coplanar arrangement (Figure 6) to facilitate the coupled proton and electron shift (PCET) from the alkoxy to the hydroxyl moiety. The corresponding relative free energy barrier is only 22.8 kcal mol^{-1} (Figure 5), yielding a water molecule, the aldehyde **15**, and two Re^{V} complexes **1**. A proton shuttle via a second methanol molecule does not reduce the activation energy, as seen before for other examples. We also checked the possibility where the alkoxy proton shifts to the oxo or the catecholate oxy moieties of the second Re instead of to the hydroxyl group, similar to the mononuclear TSs **11**−**13** and **11**−**14**, Section 2.2.3. However, all of these alternative TSs are at least by 7−13 kcal mol^{-1} higher in energy compared to the favored TS **19**−(**15** + **1**).

In consequence, among the plausible oxidation routes explored (Scheme 4), the dinuclear catalytic path from **9** via **19** directly to **15** affords by far the lowest *absolute* barrier of 32.9 kcal mol^{-1} (Figure 5).

2.2.5. Energetics with Benzyl Alcohol as Substrate. As mentioned in the Introduction, experiments were also carried out with benzyl alcohol **7a**, resulting in the product benzylaldehyde **15a**.[12] (Labels with "**a**" appended refer to analogous compounds that occur when benzyl alcohol **7a** is oxidized instead of methanol **7**, as discussed thus far. For an overview of these species, see Scheme S1 of SI.) For a selected set of intermediate structures along the favorable "dinucelar PCET" pathway for the oxidation of methanol **7** (Sections 2.2.4 and S8 of SI), we explored analogous complexes with benzyl alcohol **7a** as substrate, to examine the effect of the alcohol on the oxidation process and its energetics.

Thermodynamically, the overall change in free energy for the reaction to yield benzaldehyde **15a** from benzyl alcohol **7a** is −15.9 kcal mol^{-1}. Thus, the transformation of benzyl alcohol is more exergonic by −11.5 kcal mol^{-1} than the oxidation of methanol **7** to formaldehyde **15** (Figure S9 of SI). Intermediates **9a** and **10a** lie at free energies of 13.0 kcal mol^{-1} and 12.9 kcal mol^{-1}, respectively (i.e., they are by 6.7 kcal mol^{-1} and 2.7 kcal mol^{-1} higher than their congeners **9** and **10**). This more endergonic character seems to reflect a more crowded bonding situation in the case of benzyl alcohol. Yet, the crucial *relative* barrier **19a** → (**15a** + **1**), 18.9 kcal mol^{-1}, is even lower by 3.9 kcal mol^{-1}, than the barrier of the analogous reaction of methanol. The corresponding value of the *absolute* barrier, 31.8 kcal mol^{-1}, is also reduced compared to methanol as substrate, but only by 1.1 kcal mol^{-1}. Intermediate **11a**, at 33.0 kcal mol^{-1}, is also calculated slightly more endergonic with respect to the reactants than its methanol-derived analogue, at 30.2 kcal mol^{-1}. In summary, the oxidation of benzyl alcohol and the reduction Re^{VII} → Re^{V} are both thermodynamically and kinetically favored over the analogous transformations with methanol as substrate.

3. CONCLUSIONS

In the present computational study, we examined (i) the mechanism of O_2 activation at the metal center of the complex $[Re^{V}(O)(cat)_2]^-$, with catechol (cat) playing a crucial role as redox-active ligand, and (ii) alcohol oxidation catalyzed by the resulting oxidation product, $[Re^{VII}(O)_2(cat)_2]^-$. Combining both steps yields a catalytic cycle. These processes involve radical species and the association of mononuclear species to dinuclear complexes that are crucial both for O_2 splitting and alcohol oxidation. In view of the charged intermediates, we reported free energy values for species in methanol as solvent where the calculated entropy contributions were suitably adjusted. In addition, the energies of open-shell singlet states were corrected for spin contamination.

We successfully addressed several open issues of O_2 activation by the rhenium catechol complex, in particular the initial isomerization and the solvent effects of the charged intermediates. In the presence of O_2, the *trans*−*cis* isomerization barrier is reduced from 26.1 kcal mol^{-1}, calculated for systems in the gas phase, to 10.8 kcal mol^{-1} in methanol as solvent. With the large solvation energy of the dianionic dinuclear peroxo complex, one is able to rationalize the rather accessible energy barrier of the association step, 14.8 kcal mol^{-1}, in methanol. The calculated consecutive barriers in methanol, 10.8 kcal mol^{-1} and 14.8 kcal mol^{-1}, are compatible with the experimental finding of a two-step process of comparable barriers. Thus, the computational model presented in the current work offers a convincing rationalization of the kinetics in solution for O_2 homolysis by the oxorhenium(V) complex $[Re^{V}(O)(cat)_2]^-$ with redox-active catecholate ligands.

The main issue regarding the catalytic alcohol oxidation (i.e., the second half of the catalytic cycle) is whether it involves an accessible seven-coordinated hydroxo−alkoxo species as active oxidant, as previously suggested on the basis of experiments.[12] According to our computational work, a dinuclear cooperative pathway, including a di-Re complex in a triplet state, is the only one with a plausible energetics for the alcohol oxidation. For methanol oxidation, we calculated the corresponding highest *absolute* barrier, 33 kcal mol^{-1}, to be associated with proton-coupled electron transfer (PCET). Similar to the dinuclear peroxo dimer in the O_2 homolysis process, the redox-active ligand catechol serves as e^- buffer in the oxidation with a di-Re complex in a triplet state. For benzyl alcohol, a slightly lower absolute barrier was calculated for the dinuclear PCET catalysis than for methanol as substrate, while the overall reaction becomes notably more exergonic, from −4 kcal mol^{-1} to −16 kcal mol^{-1}.

For parallel routes via the aforementioned seven-coordinated oxidant, we calculated much higher barriers, thus effectively ruling out this hydroxo−alkoxo species **11** as viable intermediate. In fact, the highest *absolute* barriers for a path involving an intramolecular alkoxy transfer in a dinuclear complex was calculated at 51 kcal mol^{-1}, but complex **11** is also accessible via direct association of the substrate and the oxidant, over an *absolute* barrier of 33 kcal mol^{-1}. However, the subsequent oxidation of the alcohol occurs along a path involving mononuclear PCET with an *absolute* barrier of at least 46 kcal mol^{-1}.

In summary, with our computational model, we are able to rationalize the complete scenario of the experimentally studied catalytic alcohol oxidation by the complex $[Re^{V}(O)(cat)_2]^-$ where the redox-active ligand catechol plays a crucial role in

DOI: 10.1021/acscatal.5b00509
ACS Catal. 2015, 5, 4869−4880

both phases of the catalytic cycle, as e^- buffer in O_2 homolysis as well as in a dinuclear PCET step to oxidize the substrate. We suggested a detailed mechanism that should be useful for making better use of ubiquitous aerial oxygen as cheap oxidant, maybe even by complexes of more common transition metals than rhenium.

4. COMPUTATIONAL DETAILS

Full geometry optimizations, without any symmetry constraints, were carried out using the hybrid density functional theory (DFT) method B3LYP[56] as implemented in the program suite Gaussian 09, revision A.02.[57] For systems with unpaired electrons, we used the spin unrestricted Kohn−Sham (UKS) approach. SCF cycles were converged until the root-mean-square value of the changes in the density matrix was less than 10^{-8} au and the maximum change was below 10^{-6} au. The Stuttgart-Dresden effective core potential MWB60[58] and the corresponding basis set were invoked for Re; for the remaining elements, 6-31G(d,p) basis sets were employed.[59] All structures reported were subject of a normal-mode vibrational analysis, calculated at the same level of theory as the corresponding geometry optimization. All stationary points on the potential energy surface are either local minima with no imaginary vibrational frequency or transition states with exactly one imaginary frequency. Intermediate structures connected by a given transition state were confirmed by calculating the internal reaction coordinate (IRC). Unless otherwise stated, we report Gibbs free energies with adjusted entropy contributions for systems in solution; see Section 4.1. The total spin density plots were obtained from Mulliken population analyses using an isovalue of 0.006 *e*.

Solvent effects were accounted for with the conductor-like polarizable continuum model (CPCM). Geometry optimizations of systems in solution were started from stationary structures obtained for optimized structures of systems in the gas phase.[60,61] The solvation energies were calculated in methanol (ε = 32.6). For comparison, we also tested three other solvent models, IEFPCM,[60] SMD,[62] and the Onsager method,[60] as provided in Gaussian 09; the corresponding results are shown in Table S9 of SI.

4.1. Free Energies with Corrected Entropy Contributions for Systems in Solution. Calculating free energies of molecules in solution is known to be challenging due to the difficulties in estimating the corresponding entropy contribution.[63] A relatively simple, yet efficient method for estimating solvation entropies was proposed by Wertz.[64] The procedure comprises three steps, and the corresponding formula have been described in detail elsewhere[65] and are provided in Section S10 of SI. The absolute entropy of methanol in the gas phase and in solution were taken from the literature.[66] Accordingly, we calculated the Gibbs free energy of a molecular system in methanol at room temperature, 298 K, by adding the entropy correction in methanol, ΔS_m, to the entropy calculated for the system in the gas phase; see Table S10 of SI.

4.2. Diradical Species. The KS approach to DFT relies on a wave function in the form of a single determinant; the corresponding spin orbitals are calculated self-consistently when solving the Kohn−Sham equations. Closed-shell systems and some open-shell systems are well described by this approach. For instance, the triplet states of many compact molecules are readily described by spin orbitals obtained in a UKS calculation. The corresponding KS determinant in general is not an eigenstate of the total spin operator S^2, but only of the spin projection S_z, with quantum number M_S = 1. In contrast, the calculation of open-shell singlets (OSS) is problematic in the UKS formalism as the corresponding KS single-determinant wave function contains a contaminating admixture of a triplet spin state. In other words, the UKS determinant fails to describe an OSS.[67]

In the context of the present study, we were interested in a procedure that delivers an adequate approximation to the singlet−triplet energy gap of biradical species. Several procedures have been suggested and successfully applied to this spin contamination problem. Becke[68] showed that results of UKS calculations, corrected as suggested by Noodleman,[69] agree better with experimental values for the bond distance and the dissociation energy of the chromium dimer than direct UKS results. With a related procedure Yamaguchi et al. calculated improved singlet−triplet energy gaps of diradicals.[70] Another option for describing triplet and singlet states of diradical systems is Ziegler's sum method applied to OSS states.[71] One of the simplest examples is the singlet−triplet energy splitting of O_2, calculated at 10.5 kcal mol^{-1} with the UKS formalism.[72] This result is only about half of the actual value, but a correction for spin contamination yields 20.5 kcal mol^{-1},[72] in very good agreement with experiment, 22.5 kcal mol^{-1}.[73] In the present work, we estimated the energy of OSS systems using an approximate spin correction procedure proposed by Yamaguchi et al.:[70]

$$^1E(\mathrm{SC}) = {}^1E(\mathrm{U}) + f_{sc}[{}^1E(\mathrm{U}) - {}^3E(U)], f_{sc} \approx \frac{\langle {}^1S^2\rangle(\mathrm{U})}{\langle {}^3S^2\rangle(\mathrm{U}) - \langle {}^1S^2\rangle(\mathrm{U})}$$

Here $\langle {}^\alpha S^2\rangle$ is the expectation value of the total spin in state α, ^1E(SC) the spin-corrected singlet energy, ^3E(U) the total energy of the triplet state, and ^1E(U) is the single-point energy of the singlet state at the optimized geometry of the triplet state. The spin-correction procedure of Yamaguchi et al.[70] and Ziegler's sum method[71] provide very similar results, with the singlet−triplet energy difference of O_2 differing by less than 1 kcal mol^{-1}.

■ ASSOCIATED CONTENT

Supporting Information

The Supporting Information is available free of charge on the ACS Publications website at DOI: 10.1021/acscatal.5b00509.

Energies and free energies of species in gas phase and in methanol; discussion of complex **2**; structures of all stationary points; spin densities and SOMOs for species of interest; scheme and free energy profile for the reaction with benzyl alcohol; discussion of a TD-DFT study of intermediates of alcohol oxidation; tables with results for various solvation approaches; relative reaction barriers (PDF)

Cartesian coordinates of all stationary points (ZIP)

■ AUTHOR INFORMATION

Corresponding Author

*E-mail: roesch@mytum.de.

Notes

The authors declare no competing financial interest.

■ ACKNOWLEDGMENTS

We thank Dr. Zhao Jin, National University of Singapore, for stimulating discussions. We acknowledge generous computing

DOI: 10.1021/acscatal.5b00509
ACS Catal. 2015, 5, 4869−4880

resources provided by the A*STAR Computational Resource Centre.

REFERENCES

(1) Chirik, P. J.; Wieghardt, K. *Science* **2010**, *327*, 794−795.
(2) Luca, O. R.; Crabtree, R. H. *Chem. Soc. Rev.* **2013**, *42*, 1440−1459.
(3) Praneeth, V. K.; Ringenberg, M. R.; Ward, T. R. *Angew. Chem., Int. Ed.* **2012**, *51*, 10228−10234.
(4) Lyaskovskyy, V.; de Bruin, B. *ACS Catal.* **2012**, *2*, 270−279.
(5) Chirik, P. J. *Inorg. Chem.* **2011**, *50*, 9737−9740.
(6) Annibale, V. T.; Song, D. *RSC Adv.* **2013**, *3*, 11432−11449.
(7) Hindson, K.; de Bruin, B. *Eur. J. Inorg. Chem.* **2012**, *2012*, 340−342.
(8) Blackmore, K. J.; Lal, N.; Ziller, J. W.; Heyduk, A. F. *J. Am. Chem. Soc.* **2008**, *130*, 2728−2729.
(9) Trovitch, R. J.; Lobkovsky, E.; Bill, E.; Chirik, P. J. *Organometallics* **2008**, *27*, 1470−1478.
(10) Sylvester, K. T.; Chirik, P. J. *J. Am. Chem. Soc.* **2009**, *131*, 8772−8774.
(11) Yu, R. P.; Darmon, J. M.; Milsmann, C.; Margulieux, G. W.; Stieber, S. C. E.; DeBeer, S.; Chirik, P. J. *J. Am. Chem. Soc.* **2013**, *135*, 13168−13184.
(12) Lippert, C. A.; Riener, K.; Soper, J. D. *Eur. J. Inorg. Chem.* **2012**, *2012*, 554−561.
(13) Mirica, L. M.; Ottenwaelder, X.; Stack, T. D. P. *Chem. Rev.* **2004**, *104*, 1013−1046.
(14) Rolle, C. J.; Hardcastle, K. I.; Soper, J. D. *Inorg. Chem.* **2008**, *47*, 1892−1894.
(15) Smith, A. L.; Hardcastle, K. I.; Soper, J. D. *J. Am. Chem. Soc.* **2010**, *132*, 14358−14360.
(16) Dzik, W. I.; Xu, X.; Zhang, X. P.; Reek, J. N.; de Bruin, B. *J. Am. Chem. Soc.* **2010**, *132*, 10891−10902.
(17) Olatunji-Ojo, O. A.; Cundari, T. R. *Inorg. Chem.* **2013**, *52*, 8106−8113.
(18) Kim, K.; Kishima, T.; Matsumoto, T.; Nakai, H.; Ogo, S. *Organometallics* **2012**, *32*, 79−87.
(19) Yao, S.; Driess, M. *Acc. Chem. Res.* **2011**, *45*, 276−287.
(20) Tshuva, E. Y.; Lippard, S. J. *Chem. Rev.* **2004**, *104*, 987−1012.
(21) Rosenthal, J.; Nocera, D. G. *Acc. Chem. Res.* **2007**, *40*, 543−553.
(22) Ikeda, A.; Hoshino, K.; Komatsuzaki, H.; Satoh, M.; Nakazawa, J.; Hikichi, S. *New J. Chem.* **2013**, *37*, 2377−2383.
(23) Korendovych, I. V.; Kryatov, S. V.; Rybak-Akimova, E. V. *Acc. Chem. Res.* **2007**, *40*, 510−521.
(24) Bochevarov, A. D.; Li, J.; Song, W. J.; Friesner, R. A.; Lippard, S. J. *J. Am. Chem. Soc.* **2011**, *133*, 7384−7397.
(25) Tinberg, C. E.; Lippard, S. J. *Acc. Chem. Res.* **2011**, *44*, 280−288.
(26) Usharani, D.; Janardanan, D.; Li, C.; Shaik, S. *Acc. Chem. Res.* **2012**, *46*, 471−482.
(27) Nam, W. *Acc. Chem. Res.* **2007**, *40*, 465−465.
(28) Krüger, H.-J. In *Biomimetic oxidations catalyzed by transition metal complexes*, 6th ed.; Meunier, B., Eds.; Imperial College Press: London, 2000; p 363.
(29) Que, L.; Tolman, W. B. *Nature* **2008**, *455*, 333−340.
(30) Meunier, B.; De Visser, S. P.; Shaik, S. *Chem. Rev.* **2004**, *104*, 3947−3980.
(31) Valdez, C. E.; Smith, Q. A.; Nechay, M. R.; Alexandrova, A. N. *Acc. Chem. Res.* **2014**, *47*, 3110−3117.
(32) Ray, K.; Petrenko, T.; Wieghardt, K.; Neese, F. *Dalton Trans.* **2007**, 1552−1566.
(33) Kampa, M.; Lubitz, W.; van Gastel, M.; Neese, F. *JBIC, J. Biol. Inorg. Chem.* **2012**, *17*, 1269−1281.
(34) Hachmann, J.; Frazier, B. A.; Wolczanski, P. T.; Chan, G. K. *ChemPhysChem* **2011**, *12*, 3236−3244.
(35) Paretzki, A.; Bubrin, M.; Fiedler, J.; Záliš, S.; Kaim, W. *Chem. - Eur. J.* **2014**, *20*, 5414−5422.
(36) Bittner, M. M.; Lindeman, S. V.; Popescu, C. V.; Fiedler, A. T. *Inorg. Chem.* **2014**, *53*, 4047−4061.
(37) Hojilla Atienza, C. C.; Milsmann, C.; Semproni, S. P.; Turner, Z. R.; Chirik, P. J. *Inorg. Chem.* **2013**, *52*, 5403−5417.
(38) Darmon, J. M.; Stieber, S. C. E.; Sylvester, K. T.; Fernández, I.; Lobkovsky, E.; Semproni, S. P.; Bill, E.; Wieghardt, K.; DeBeer, S.; Chirik, P. J. *J. Am. Chem. Soc.* **2012**, *134*, 17125−17137.
(39) Sharma, S.; Sivalingam, K.; Neese, F.; Chan, G. K.-L. *Nat. Chem.* **2014**, *6*, 927−933.
(40) Lippert, C. A.; Arnstein, S. A.; Sherrill, C. D.; Soper, J. D. *J. Am. Chem. Soc.* **2010**, *132*, 3879−3892.
(41) da Silva, J. A. L.; Fraústo da Silva, J. J. R.; Pombeiro, A. J. L. *Coord. Chem. Rev.* **2011**, *255*, 2232−2248.
(42) Velusamy, S.; Ahamed, M.; Punniyamurthy, T. *Org. Lett.* **2004**, *6*, 4821−4824.
(43) Biradar, A. V.; Dongare, M. K.; Umbarkar, S. B. *Tetrahedron Lett.* **2009**, *50*, 2885−2888.
(44) Sousa, S. C.; Bernardo, J. R.; Florindo, P. R.; Fernandes, A. C. *Catal. Commun.* **2013**, *40*, 134−138.
(45) Zapata-Rivera, J.; Caballol, R.; Calzado, C. J. *Phys. Chem. Chem. Phys.* **2011**, *13*, 20241−20247.
(46) Haack, P.; Limberg, C.; Ray, K.; Braun, B.; Kuhlmann, U.; Hildebrandt, P.; Herwig, C. *Inorg. Chem.* **2011**, *50*, 2133−2142.
(47) Aboelella, N. W.; Kryatov, S. V.; Gherman, B. F.; Brennessel, W. W.; Young, V. G.; Sarangi, R.; Rybak-Akimova, E. V.; Hodgson, K. O.; Hedman, B.; Solomon, E. I. *J. Am. Chem. Soc.* **2004**, *126*, 16896−16911.
(48) Landis, C. R.; Morales, C. M.; Stahl, S. S. *J. Am. Chem. Soc.* **2004**, *126*, 16302−16303.
(49) Keith, J. M.; Nielsen, R. J.; Oxgaard, J.; Goddard, W. A. *J. Am. Chem. Soc.* **2005**, *127*, 13172−13179.
(50) Popp, B. V.; Wendlandt, J. E.; Landis, C. R.; Stahl, S. S. *Angew. Chem., Int. Ed.* **2007**, *46*, 601−604.
(51) Harvey, J. N.; Aschi, M. *Phys. Chem. Chem. Phys.* **1999**, *1*, 5555−5563.
(52) Koseki, S.; Hisashima, T.-a.; Asada, T.; Toyota, A.; Matsunaga, N. *J. Chem. Phys.* **2010**, *133*, 174112−174119.
(53) Edwards, C. F.; Griffith, W. P.; White, A. J.; Williams, D. J. *J. Chem. Soc., Dalton Trans.* **1992**, 957−962.
(54) Tadokoro, M.; Inoue, T.; Tamaki, S.; Fujii, K.; Isogai, K.; Nakazawa, H.; Takeda, S.; Isobe, K.; Koga, N.; Ichimura, A.; Nakasuji, K. *Angew. Chem., Int. Ed.* **2007**, *46*, 5938−5942.
(55) Deng, L.; Ziegler, T. *Organometallics* **1997**, *16*, 716−724.
(56) Kohn, W.; Becke, A. D.; Parr, R. G. *J. Phys. Chem.* **1996**, *100*, 12974−12980.
(57) Frisch, M. J.; Trucks, G. W.; Schlegel, H. B.; Scuseria, G. E.; Robb, M. A.; Cheeseman, J. R.; Scalmani, G.; Barone, V.; Mennucci, B.; Petersson, G. A.; Nakatsuji, H.; Caricato, M.; Li, X.; Hratchian, H. P.; Izmaylov, A. F.; Bloino, J.; Zheng, G.; Sonnenberg, J. L.; Hada, M.; Ehara, M.; Toyota, K.; Fukuda, R.; Hasegawa, J.; Ishida, M.; Nakajima, T.; Honda, Y.; Kitao, O.; Nakai, H.; Vreven, T.; Montgomery, J. A., Jr.; Peralta, J. E.; Ogliaro, F.; Bearpark, M.; Heyd, J. J.; Brothers, E.; Kudin, K. N.; Staroverov, V. N.; Kobayashi, R.; Normand, J.; Raghavachari, K.; Rendell, A.; Burant, J. C.; Iyengar, S. S.; Tomasi, J.; Cossi, M.; Rega, N.; Millam, M. J.; Klene, M.; Knox, J. E.; Cross, J. B.; Bakken, V.; Adamo, C.; Jaramillo, J.; Gomperts, R.; Stratmann, R. E.; Yazyev, O.; Austin, A. J.; Cammi, R.; Pomelli, C.; Ochterski, J. W.; Martin, R. L.; Morokuma, K.; Zakrzewski, V. G.; Voth, G. A.; Salvador, P.; Dannenberg, J. J.; Dapprich, S.; Daniels, A. D.; Farkas, Ö.; Foresman, J. B.; Ortiz, J. V.; Cioslowski, J.; Fox, D. J. *Gaussian 09*, Revision A.02, Gaussian, Inc.: Wallingford CT, 2009.
(58) Andrae, D.; Häußermann, U.; Dolg, M.; Stoll, H.; Preuss, H. *Theor. Chim. Acta* **1990**, *77*, 123−141.
(59) Binkley, J. S.; Pople, J. A.; Hehre, W. J. *J. Am. Chem. Soc.* **1980**, *102*, 939−947.
(60) Tomasi, J.; Mennucci, B.; Cammi, R. *Chem. Rev.* **2005**, *105*, 2999−3094.
(61) Tomasi, J.; Persico, M. *Chem. Rev.* **1994**, *94*, 2027−2094.
(62) Marenich, A. V.; Cramer, C. J.; Truhlar, D. G. *J. Phys. Chem. B* **2009**, *113*, 6378−6396.

DOI: 10.1021/acscatal.5b00509
ACS Catal. 2015, 5, 4869−4880

(63) Ho, J.; Klamt, A.; Coote, M. L. *J. Phys. Chem. A* **2010**, *114*, 13442−13444.
(64) Wertz, D. H. *J. Am. Chem. Soc.* **1980**, *102*, 5316−5322.
(65) Cooper, J.; Ziegler, T. *Inorg. Chem.* **2002**, *41*, 6614−6622.
(66) Lide, D. R. In *CRC Handbook of chemistry and physics*; Internet Version 2005, CRC Press: Boca Raton, 2005; p 5−28.
(67) Gräfenstein, J.; Kraka, E.; Filatov, M.; Cremer, D. *Int. J. Mol. Sci.* **2002**, *3*, 360−394.
(68) Edgecombe, K. E.; Becke, A. D. *Chem. Phys. Lett.* **1995**, *244*, 427−432.
(69) Noodleman, L.; Davidson, E. R. *Chem. Phys.* **1986**, *109*, 131−143.
(70) Yamaguchi, K.; Jensen, F.; Dorigo, A.; Houk, K. N. *Chem. Phys. Lett.* **1988**, *149*, 537−542.
(71) Ziegler, T.; Rauk, A.; Baerends, E. *Theor. Chim. Acta* **1977**, *43*, 261−271.
(72) Xu, X.; Goddard, W. A. *Proc. Natl. Acad. Sci. U. S. A.* **2002**, *99*, 15308−15312.
(73) Herzberg, G. In *Molecular spectra and molecular structure, Spectra of diatomic molecules*; 2nd ed.; D. Van Nostrand Company, Inc.: New York, 1965; Vol. *1*, p 560.

DOI: 10.1021/acscatal.5b00509
ACS Catal. 2015, 5, 4869−4880